

# A new photonic crystal fiber gas sensor with a hexagonal microstructure core suitable for a wide range of wavelengths

ARYAN ABBASZADEH, SOMAYEH MAKOUEI\*, SAEED MESHGINI

Faculty of Electrical and Computer Engineering, University of Tabriz, Tabriz, 51664, Iran

A photonic crystal fiber gas sensor is proposed, which gives the highest sensitivity for the wide range of 1.1 $\mu$ m to 1.7 $\mu$ m. The numerical investigation for analyzing the optical properties is calculated by the finite element method. The simulation results show that the proposed PCF gives high relative sensitivity as high as 74.53% and high birefringence of  $2.1 \times 10^{-2}$  and effective area of 5.47 $\mu$ m<sup>2</sup> and low confinement loss  $4.37 \times 10^{-2}$  dB/m at the wavelength of  $\lambda=1.33\mu$ m. The variation of diameter of holes is investigated, and the result shows that this structure shows good resistance for errors from fabrication processes.

(Received January 13, 2021; accepted November 24, 2021)

*Keywords:* Photonic crystal fiber, Gas sensor, Relative sensitivity, Confinement loss

## 1. Introduction

Photonic crystal fibers (PCFs) are a new type of optical fiber that can overcome some restrictions of traditional optical fibers because of their asymmetric geometry. These fibers consist of periodic layers of holes that spread along with the entire fiber [1]. PCFs can be divided into two categories. One of them is the photonic band-gap (PBG), which the light is guided by the band-gap role [2]. Another is index-guiding (IG) PCF, which light is guided by the total internal reflection like the traditional fibers [3]. Hollow-core (HC) PCFs emit light by using PBG effects [4]. Because in this type of PCF, light interacts with more gases in the core region, they are more suitable for sensing applications [5-7]. Recently, the HC PCFs have been proposed for several applications such as liquid sensors [8], gas sensors [9, 10], humidity sensors [11]. Some important parameters are used for investigating the performance of different PCFs. These optical properties are high relative sensitivity [12], low confinement loss [13], high effective area [14], high birefringence, and high nonlinearity [15]. PCFs with different geometries can change these optical attributes. Researchers are looking for designing PCFs, which give the highest relative sensitivity and low confinement loss simultaneously. They have suggested many PCFs with different geometries such as octagonal [16], hexagonal [17], elliptical [18], decagonal [19], and circular honeycomb [20] cladding layers to improve sensing attributes. The spectroscopy gas sensor based on PCFs depends on how much gases interact with light in the core region [21]. Therefore, if the designed PCF gives high relative sensitivity for a wide range of wavelengths, the PCF can detect various gases. Table.1 shows the absorption wavelength and line strength of some gases [22, 23].

Table 1. The absorption wavelength and line strength of some gases [22, 23]

Gas	Absorption wavelength ( $\mu$ m)	Line strength ( $\text{cm}^{-2}\text{atm}^{-1}$ )
Acetylene (C <sub>2</sub> H <sub>2</sub> )	1.533	$20 \times 10^{-2}$
Hydrogen iodide (HI)	1.541	$0.775 \times 10^{-2}$
Ammonia (NH <sub>3</sub> )	1.544	$0.925 \times 10^{-2}$
Carbon monoxide (CO)	1.567	$0.0575 \times 10^{-2}$
Carbon dioxide (CO <sub>2</sub> )	1.573	$0.048 \times 10^{-2}$
Hydrogen sulfide (H <sub>2</sub> S)	1.578	$0.325 \times 10^{-2}$
Methane (CH <sub>4</sub> )	1.667, 1.33	$1.5 \times 10^{-2}$
Hydrogen fluoride (HF)	1.33	$32.5 \times 10^{-2}$
Hydrogen bromide (HBr)	1.341	$0.0525 \times 10^{-2}$

Several PCF gas sensors have been proposed to achieve high sensitivity at the wavelength of 1.33 $\mu$ m, which is in the methane absorption line for air pollution monitoring applications. Olyaei et al. [24] proposed a hexagonal PCF, which gives relative sensitivity of 13.23% at 1.33 $\mu$ m. They also showed that outer layers are mostly affected by the confinement loss, and inner layers in the cladding region are mostly affected by the relative sensitivity. Morshed [25] presented a new PCF with a microstructure core, which gives the relative sensitivity of 42.27% at  $\lambda=1.33\mu$ m. Asaduzzaman [26] proposed a new hexagonal PCF with elliptical holes in the core region. This structure gives the

relative sensitivity of 53.07% at the wavelength of  $\lambda=1.33\mu\text{m}$ . This structure also gives high birefringence and nonlinearity, which makes it more suitable for air pollution monitoring. Finally, in [12], Rabee proposed a circular PCF structure that gives a relative sensitivity as high as 72.04% at a wavelength of  $\lambda=1.33\mu\text{m}$ . This structure also gives high sensitivity for a wide range of wavelengths from  $1.1\mu\text{m}$  to  $1.7\mu\text{m}$ , making it useful for detecting gases.

In this paper, a new PCF is proposed with four circular layers in the cladding region and four hexagonal layers in the core region. The impact of variations in holes diameter on the relative sensitivity and confinement loss in the cladding and core region of the proposed PCF is investigated at the wavelength of  $1.33\mu\text{m}$ . Finally, the relative sensitivity and birefringence of the proposed PCF are compared with the gas sensors based on PCF reported in the literature at the wavelength of  $1.33\mu\text{m}$ .

## 2. Proposed PCF based geometrics

Fig.1 shows the geometry of the proposed PCF in which the cladding contains four circular layers, and the core contains four hexagonal layers with a central core that surrounded them. The diameter of the layers in the cladding region is defined by  $d$ . The diameter of the four hexagonal layers in the core region is defined by  $d_{c2}$ , and the diameter of the central hole is defined by  $d_{c1}$ . The corresponding angles between air holes in each ring in the cladding region from outside to inside are  $12^\circ$ ,  $15^\circ$ ,  $20^\circ$ , and  $30^\circ$ , respectively. The distance of the layer with the other next close layer in the cladding region is  $1.1\mu\text{m}$ . The distance between the centers of two adjacent holes is called the pitch. The distance between hexagonal holes in the core region is represented by  $A_{c1}$ . Table.2 shows the value of these parameters. The perfectly matched layer is adjusted around 10% of the entire PCF diameter for absorbing the light-wave [26].

Table 2. The value of the proposed PCF parameters

parameter	$d$	$d_{c1}$	$d_{c2}$	$A_{c1}$
Value ( $\mu\text{m}$ )	1	0.28	0.3	0.32

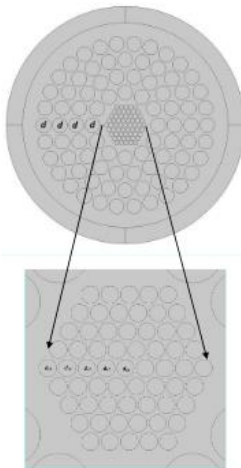


Fig. 1. The geometry of the proposed PCF

## 3. Mathematical equations

The optical properties of PCFs such as relative sensitivity, confinement loss, birefringence, and the effective area can be computed by the finite element method (FEM). Many complex structures can be solved by FEM [26]. The confinement loss is one of the critical optical properties of PCFs. When the light penetrates the core, and spread along the cladding region, this parameter will be increased. As the confinement loss is decreased, it shows that the PCFs can trap light into the core region perfectly, and less light will be leakage into the cladding region. The confinement loss can be computed by the following equation [27]:

$$L_c = 8.686 \times k_0 \times \text{Im}[n_{eff}] \left( \frac{dB}{m} \right) \quad (1)$$

Another significant parameter for obtaining the optical properties of PCFs is the relative sensitivity. This parameter shows how much gas components interact with the light at a specific wavelength [10]. The relative sensitivity of a PCF shows the sensing capability of it. By increasing this parameter, more light will be trapped in the core region, and the interaction between light and gas will be improved. Therefore, the PCF can detect more gases precisely. This parameter is incorporated with the beer-lambert law. The Beer-lambert law is expressed by the following equation:

$$I(\lambda) = I_0(\lambda) \exp(-r \alpha_m l c) \quad (2)$$

Here,  $I(\lambda)$  and  $I_0(\lambda)$  show the input and output intensities respectively,  $\alpha_m$  is the gas absorption coefficient,  $l$  is the length of the PCF,  $c$  is the gas concentration. The relative sensitivity indicates the distribution of the electromagnetic fields in the PCF. These fields are managed by the real part of refractive indexes and can be obtained from the following equation:

$$r = \frac{n_s}{\text{Re}[n_{eff}]} f \quad (3)$$

Here,  $\text{Re}[n_{eff}]$  is the real part of the effective mode index, and  $n_s$  is the refractive index of gas species considered 1; the coefficient  $f$  is the ratio of holes power to total power, which can be defined as [28]:

$$f = \frac{\int_{hole} \text{Re}(E_x H_y - E_y H_x) dx dy}{\int_{total} \text{Re}(E_x H_y - E_y H_x) dx dy} \quad (4)$$

Here,  $E_x$  and  $E_y$  are the transverse electric fields, besides  $H_x$  and  $H_y$  are the transverse magnetic fields of mode.

Birefringence is one of the crucial properties of PCFs. This parameter depends on the asymmetry of the air holes [23]. This parameter is computed by subtraction of the x

polarization and y polarization of the refractive index, which can be defined [23]:

$$B = |n_x - n_y| \tag{5}$$

The effective area is an area that light is emitted from the region. The electric field (E) distribution appears from the inside of the core for fundamental modes. For transferring high rate data, a more effective area is required, but a lower amount of this parameter is preferable for nonlinear applications [23]. This parameter can be specified by the following equation [29]:

$$A_{eff} = \frac{(\iint |E|^2 dx dy)^2}{\iint |E|^4 dx dy} \tag{6}$$

#### 4. Simulation results and discussion

Fig. 2a shows the 2D mode of the fundamental distribution of the electric field at the wavelength of 1.33μm. Figs. 2b and 2c show the normalized electric field distribution for two polarized modes at 1.33μm. It may be seen that the electric field is trapped in the core region for two polarized modes. The finite element method is used for analyzing numerical results. The size of the mesh is chosen as normal, which gives the number of degrees 220283. The numerical results show that the proposed PCF gives the relative sensitivity as high as 74.53%, effective area as high as 5.47μm<sup>2</sup>, and birefringence as high as 2.1×10<sup>-2</sup> at the wavelength of 1.33μm. The confinement loss of the proposed PCF is 4.37×10<sup>-2</sup> dB/m at λ=1.33μm. Fig.3a and Fig.3b show the relative sensitivity and confinement loss of proposed PCF from wavelengths 0.9μm to 1.7μm. As can be seen, the PCF shows the highest sensitivity for wavelengths from 1.3μm to 1.7μm. Therefore, this sensor can detect a wide range of gases without any variation of significant relative sensitivity. The mean and variance of the relative sensitivity from wavelength 1.3μm to 1.7μm are 73.528 and 2.1134, respectively. This information proves that the relative sensitivity can be considered relatively constant for the wide range of these wavelengths. Furthermore, According to Table 1, because the absorption line of most gases is close around wavelengths of 1.3μm to 1.5μm, it is expected that this structure can detect these gases precisely. Both relative sensitivity and confinement

loss are increased by increasing the wavelength from 1.1μm to 1.7μm.

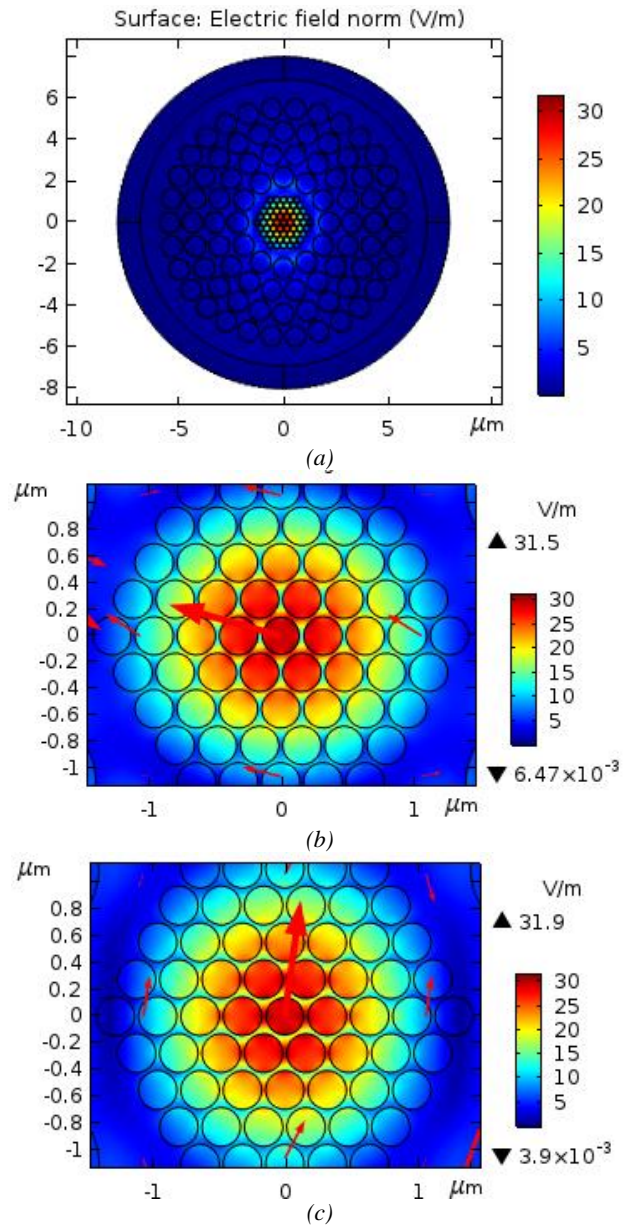


Fig. 2. The electric field distribution for the proposed PCF a) 2D view of mode field pattern. b) x-polarization c) y-polarization modes at the wavelength of 1.33μm (color online)

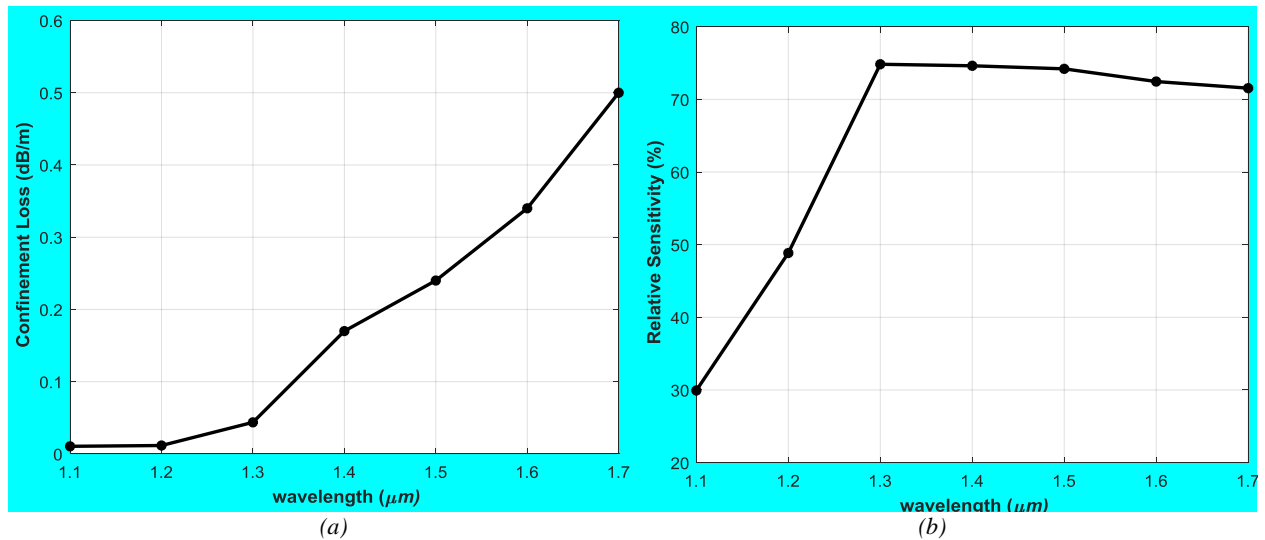


Fig. 3. a) Confinement loss of proposed PCF for the wavelength from  $1.1\mu\text{m}$  to  $1.7\mu\text{m}$  and b) The relative sensitivity (color online)

Because the variation of the diameter may change the optical properties of the proposed PCF, these variations for both the cladding and core regions should be investigated at  $\lambda=1.33\mu\text{m}$ . The  $d$ ,  $d_{c1}$ , and  $d_{c2}$  parameters have been

changed, respectively, while the other ones are kept constant. First, the variation of the  $d$  parameter in the cladding region is investigated.

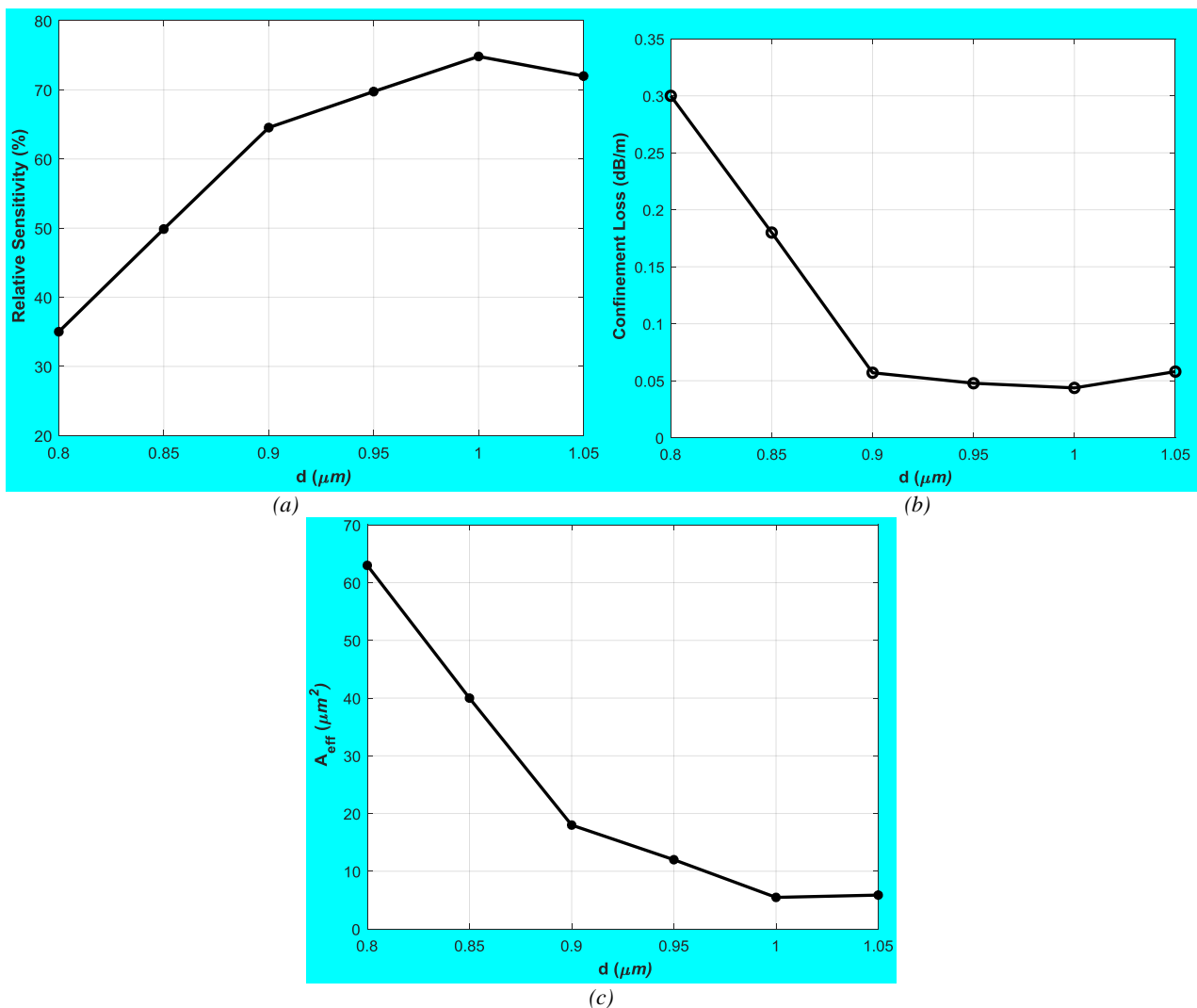


Fig. 4. Variation of the a) relative sensitivity, b) confinement loss, and c) effective area for  $d$  parameter (color online)

From Figs. 4a to 4c, it can be seen that by decreasing the  $d$  parameter from  $1\mu\text{m}$  to  $0.8\mu\text{m}$ , the relative sensitivity is decreased. When the size of holes in the cladding region is decreased, more light will be leakage to the outer layers in the cladding region and make the confinement loss and effective area is increased. The results show that this structure shows good resistance for errors less than 10%, and the relative sensitivity, confinement loss and effective area do not change rapidly. From Figs 4a to 4c, it can be seen that increasing the diameter of  $d$  parameter, makes the relative sensitivity be decreased and confinement loss and effective area be increased slightly, from  $1\mu\text{m}$  to  $1.05\mu\text{m}$ . The diameters larger than  $1.1\mu\text{m}$  are not investigated because the value of pitch is chosen  $1.1\mu\text{m}$ , and for bigger values equal to  $1.1\mu\text{m}$ , the holes will be interrupted in the cladding region.

The core region consists of four hexagonal layers that have the same diameter and are represented by the  $d_{c2}$  parameter. Figs. 5a to 5c show the relative sensitivity,

confinement loss, and effective area of the  $d_{c2}$  parameter for the variations from  $0.28\mu\text{m}$  to  $0.3\mu\text{m}$ . As can be seen from these figures, by increasing the diameters for these layers, relative sensitivity, confinement loss, and effective area are a bit changed. It may be seen that this layer is resistant to errors of less than 20%. Fig.5c shows the impact of the  $d_{c2}$  parameter on the effective area. As the diameter of these layers is increased, the space between holes is decreased, which makes the relative sensitivity is increased. The electric field will be distributed along the core region. Therefore, the effective area will be increased. From Figs 5.a to 5.c, it can be seen that, although increasing the diameter of holes from  $0.3\mu\text{m}$  to  $0.305\mu\text{m}$ , makes the relative sensitivity and effective area be increased. However, the confinement loss is also increased and makes electric field leaks to outer layers. Therefore, the optimized amount for this parameter is  $0.3\mu\text{m}$ .

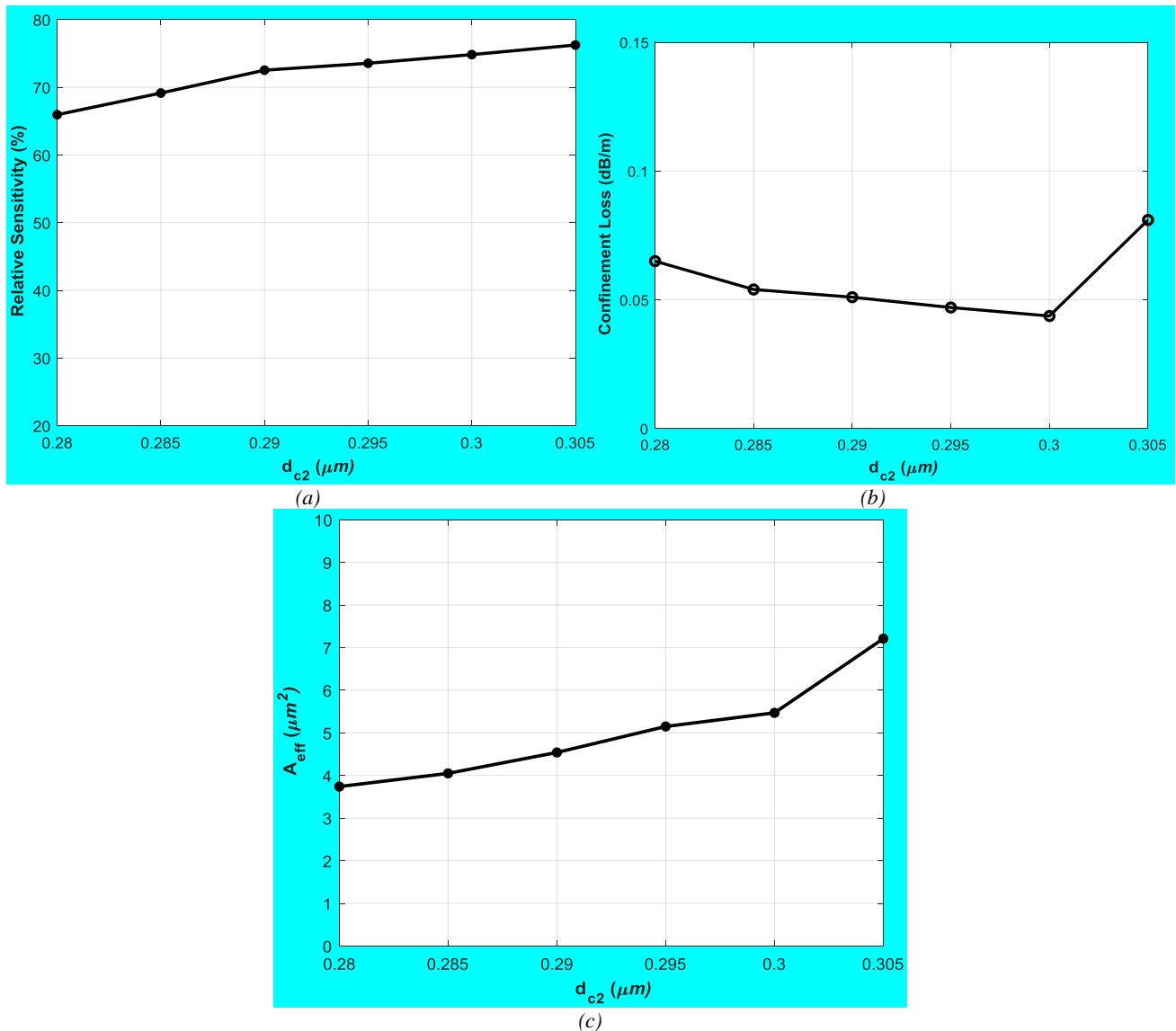


Fig. 5. Variation of the a) relative sensitivity, b) confinement loss and c) effective area for  $d_{c2}$  parameter (color online)

Finally, the variation of the central hole is investigated for the core region. Figs 6a to 6c show the impact of the variation of this parameter on the relative sensitivity, confinement loss, and effective area.

The results show that this parameter also exhibits good resistance for the variations of diameters for errors of  $\pm 20\%$ .

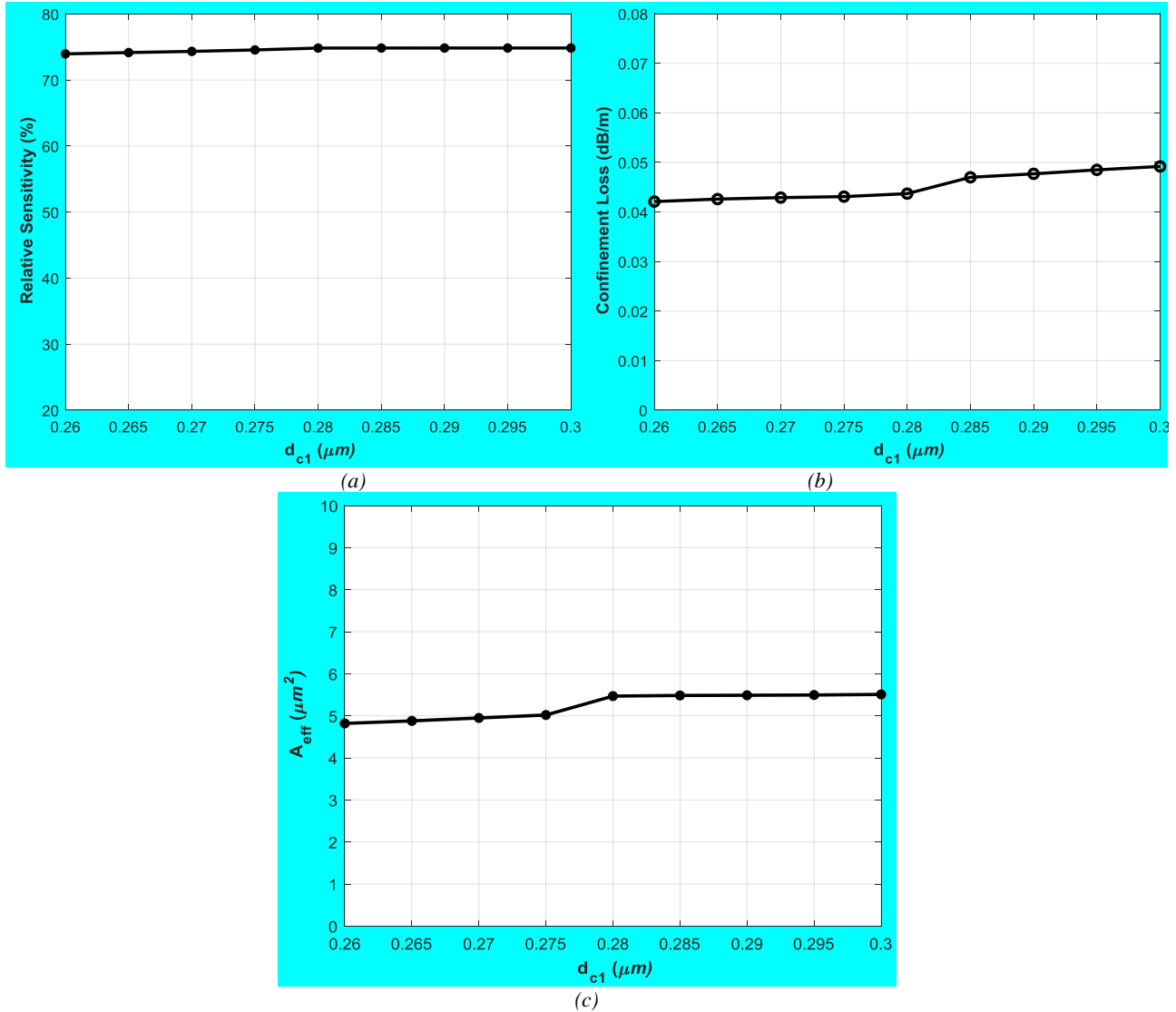


Fig. 6. Variation of the a) relative sensitivity, b) confinement loss and c) effective area for  $d_{c1}$  parameter (color online)

Table 3 shows the impact of the pitch in the cladding and core region on the relative sensitivity, confinement loss, and effective area when the size of the pitch is reduced by 10%. The parameter of the pitch in the cladding region from the inner layer to the outer layer is denoted by  $\Lambda_1$ ,  $\Lambda_2$ ,  $\Lambda_3$ , and  $\Lambda_4$ . As can be seen, reducing the distance between layers has little effect on these parameters. By reducing the pitch in the cladding region, the distance between layers is reduced and makes the relative sensitivity be increased, and the confinement loss is decreased. Because by reducing pitch, the less electric field leaks to cladding region, and

makes the relative sensitivity be increased, and the effective area is decreased. The last line of Table.3 shows the impact of the variation of pitch on relative sensitivity, confinement loss, and effective area in the core region. The results show that reducing the pitch in the core region makes the relative sensitivity be increased slightly. However, the space between the core region and the innermost layer in the cladding region is increased, and this makes a little electric field leaks to this region. Therefore, the confinement loss and effective area will be increased.

Table 3. The effect of a 10% decrease for the pitch on the relative sensitivity, confinement loss, and effective area in the cladding and core region

pitch	Relative sensitivity (%)	Confinement loss (dB/m)	Effective area ( $\mu\text{m}^2$ )
$\Lambda_1$	74.60	$5.33 \times 10^{-2}$	4.35
$\Lambda_2$	74.57	$3.25 \times 10^{-2}$	4.71
$\Lambda_3$	74.54	$2.54 \times 10^{-2}$	4.85
$\Lambda_4$	74.54	$2.17 \times 10^{-2}$	4.87
$\Lambda_{cl}$	74.89	$6.23 \times 10^{-2}$	6.28

Table 4 shows the impact of the pitch in the cladding and core region on the relative sensitivity, confinement loss, and effective area when the size of the pitch increased by 10%. As can be seen, increasing the distance between layers in the cladding region makes the relative sensitivity be decreased, and the confinement loss and effective area be increased. However, the impact of this variation is different for each layer. As can be seen, the innermost layer or  $\Lambda_1$  in the cladding region shows more changes than other layers when the pitch is increased 10%. When the distance between the first layer is increased, the space in this area is increased, and the electric field leaks to this area. Therefore, it makes the confinement loss and effective area be increased, and

the relative sensitivity is decreased. The variation of the other layers in the cladding region has little effect on relative sensitivity, confinement loss, and effective area. The last line of Table.4 shows the impact of the variation of pitch on relative sensitivity, confinement loss, and effective area in the core region. As can be seen, increasing the pitch for this parameter makes the relative sensitivity decrease to 69.72%, and confinement loss and effective area increase to  $2.3 \times 10^{-1}$  dB/m and  $21.3 \mu\text{m}^2$ , respectively. As we have seen, the results show that the proposed sensor showed good resistance to variations in diameter holes. Therefore, the sensor is stable to manufacturing errors.

Table 4 The effect of a 10% increase for the pitch on the relative sensitivity, confinement loss and effective area in the cladding and core region

Pitch	Relative sensitivity (%)	Confinement loss (dB/m)	Effective area ( $\mu\text{m}^2$ )
$\Lambda_1$	68.54	$1.23 \times 10^{-1}$	19.5
$\Lambda_2$	73.27	$5.95 \times 10^{-2}$	5.65
$\Lambda_3$	74.35	$5.74 \times 10^{-2}$	5.8
$\Lambda_4$	74.43	$5.11 \times 10^{-2}$	4.9
$\Lambda_{cl}$	69.72	$2.38 \times 10^{-1}$	21.3

Fig. 7a shows the impact of the number of circular cladding layers on the relative sensitivity. It can be seen that the structure has a bit effect on the relative sensitivity for two and three layers. But increasing layers to four make the relative sensitivity is decreased. Fig.7b shows the impact of the gas refractive index on the relative sensitivity at the

wavelength of  $1.33 \mu\text{m}$ . It may be seen that the maximum relative sensitivity for this structure reaches gas refractive index 1. Because the refractive index of most gases is close to 1 and this structure gives a peak in this area, it is expected that the proposed PCF can detect more gases with more accuracy.

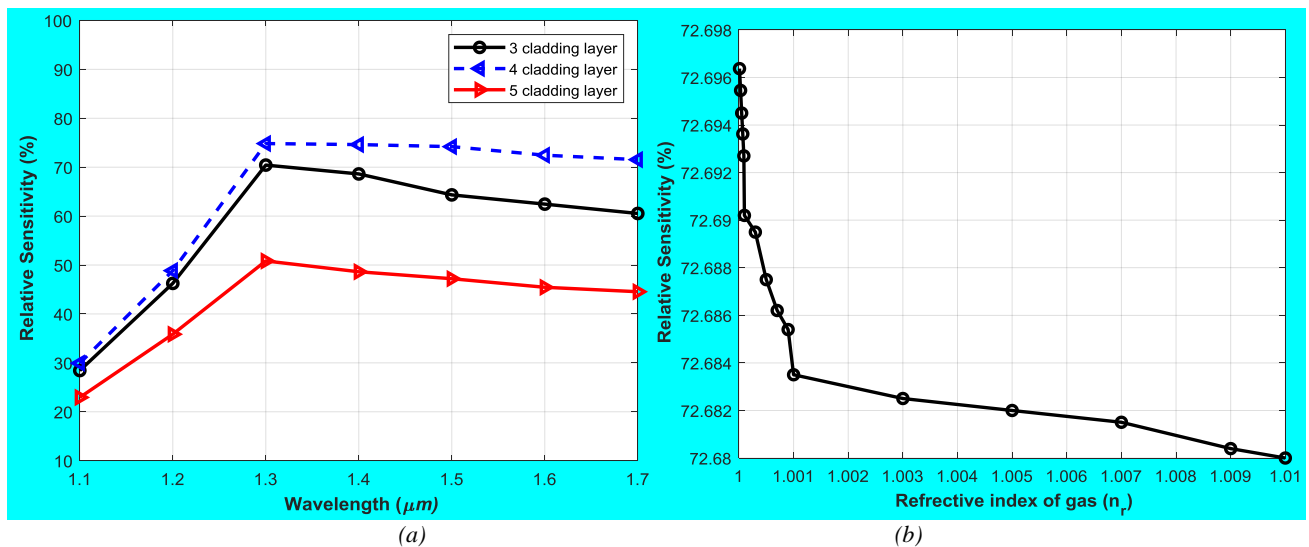


Fig. 7. a) Variation of the relative sensitivity from the wavelength of 1.1 to 1.7 using 3, 4, and 5 circular cladding b) Variation of the relative sensitivity with the gas refractive index (color online)

Table 5 exhibits a comparison between the proposed PCF and those reported in the literature. It may be seen that the suggested PCF has more relative sensitivity and high birefringence than the other PCFs reported for the gas sensor at the wavelength of  $\lambda=1.33\mu\text{m}$ . If the diameter of holes in the cladding and core region is chosen the same and the number of the layer be less, the fabrication process will be easier. Two outer layers of cladding in the [23, 24] are bigger than other layers, and the number of cladding layers is five. In [25], the structure of cladding is chosen equaled,

and the number of the layer in the cladding is five, although the sensitivity is not still very high. In [12], the diameter of the cladding layers is equaled, and the structure gives high sensitivity at  $1.33\mu\text{m}$ . Furthermore, the number of cladding is five. The diameter of holes in the cladding region has the same sizes, and the number of cladding is four for the PCF proposed in this paper. Therefore, the proposed PCF has a simple structure than the PCF presented in [12], which makes the fabrication process be facile.

Table 5 Comparison of the relative sensitivity and birefringence of proposed PCF with those reported in the literature at  $\lambda=1.33\mu\text{m}$

Ref	Relative sensitivity (%)	birefringence
[24]	13.25	-
[25]	42.27	-
[26]	53.07	$6.9 \times 10^{-3}$
[12]	72.04	-
Proposed PCF	74.53	$2.1 \times 10^{-2}$

The spectroscopy system can be used for practical work to measure the different concentrations of gases [30]. This method consists of a laser, a filter to transmit only the absorption wavelength of a specific gas, a chamber gas with a PCF, a detector to convert the light to an electrical signal, and a PC to show the results. Ammonia is a toxic gas that can be harmful to human health and the environment [31]. Therefore, detection of this gas can be vital in industrial environments. The absorption line of the ammonia gas is at the wavelength of  $1.544\mu\text{m}$ . Fig.8 shows the relative sensitivity of the proposed PCF when the ammonia gas is filled with a low concentration from  $1 \times 10^{-4} \text{ kg/m}^3$  to  $1 \times 10^{-3} \text{ kg/m}^3$ . The temperature and pressure are chosen at  $34^\circ\text{C}$  and  $1\text{atm}$ , respectively. As can be seen, when the core region fills with ammonia gas, it still gives high sensitivity of 61%.

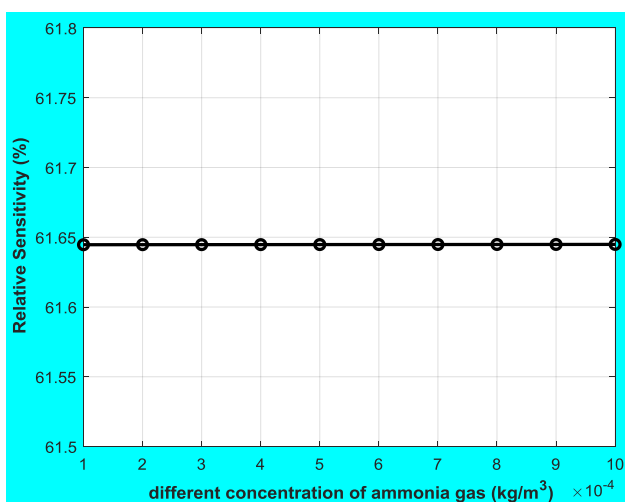


Fig. 8. Variation of the relative sensitivity from different concentration of ammonia gas at  $\lambda=1.544\mu\text{m}$  (color online)

The process of fabrication for PCFs is an important issue. The proposed PCF has circular layers in the cladding region and hexagonal layers in the core region. The

fabrication of the core region may not be easy because of microstructure holes. But some nanotechnology techniques can overcome this challenge. Several techniques have been proposed for the fabrication of PCFs, such as drilling [32], stack and draw [33], extrusion [34], and sol-gel casting [35]. The last method is more suitable for designing microstructure in the core region. Therefore, the sol-gel method can be used for fabricating the proposed PCF.

## 5. Conclusion

A new PCF gas sensor is proposed, which gives high sensitivity for the wavelength from  $1.1\mu\text{m}$  to  $1.7\mu\text{m}$ . The results showed that the suggested PCF gives the relative sensitivity as high as 74.53%, high birefringence of  $2.1 \times 10^{-2}$ , the effective area of  $5.47\mu\text{m}^2$ , and low confinement loss of  $4.37 \times 10^{-2} \text{ dB/m}$  at the wavelength of  $\lambda=1.33\mu\text{m}$ . The variation of the diameters for both cladding and core region is investigated. The results showed that the proposed PCF indicates good resistance to the errors of fabrication.

## References

- [1] P. Russell, *Science* **299**, 358 (2003).
- [2] J. C. Knight, J. Broeng, T. A. Birks, P. S. J. Russell, *Science* **282**, 1476 (1998).
- [3] J. C. Knight, T. A. Birks, P. S. J. Russell, D. M. Atkin, *Optics Letters* **21**, 1547 (1996).
- [4] F. Couny, F. Benabid, P. S. Light, *Optics Letters* **31**, 3574 (2006).
- [5] G. Humbert, J. C. Knight, G. Bouwmans, P. S. J. Russell, D. P. Williams, P. J. Roberts, J. Mangan, *Opt. Express* **12**, 1477 (2004).
- [6] C. Rohit, S. Avtar, B. Randhir, 13th International Conference on Fiber Optics and Photonics, W3A.75 (2016).
- [7] Ruwei Yu, Yuxing Chen, Lingling Shui, L. Xiao, *Sensors* **20**, (2020).

- [8] Z. Tan, X. Li, Y. Chen, P. Fan, *Plasmonics* **9**, 167 (2014).
- [9] L. Zhang, G.-J. Ren, J.-Q. Yao, *Optoelectronics Letters* **9**, 438 (2013).
- [10] Md. Ranju Sardar, M. Faisal, *Journal of Sensor Technology* **9**, 12 (2019).
- [11] W. Getinet, F. Andrea, M. Christos, S. Alessio, K. R. Henrik, B. Ole, *Opt. Mater. Express* **7**, 286 (2017).
- [12] A. S. H. Rabee, M. F. O. Hameed, A. M. Heikal, S. S. A. Obayya, *Optik* **188**, 78 (2019).
- [13] Shahli Tabassum, Shahiruddin, Dharmendra K. Sing, M. A. Hassan, *Optical and Wireless Technologies* **546**, 271 (2020).
- [14] M. Niels Asger, *Opt. Express* **10**, 341 (2002).
- [15] Y. Tianyu, W. Erlei, J. Haiming, H. Zhijia, X. Kang, *Opt. Express* **23**, 8329 (2015).
- [16] K. Ahmed, M. Morshed, S. Asaduzzaman, M. F. H. Arif, *Optik* **131**, 687 (2017).
- [17] F. Begum, Y. Namihira, S. M. Abdur Razzak, S. Kaijage, N. H. Hai, T. Kinjo, et al., *Optics Communications*, **282**, 1416 (2009).
- [18] R. Hao, Z. Li, G. Sun, L. Niu, Y. Sun, *Optical Fiber Technology* **19**, 363 (2013).
- [19] S. M. A. Razzak, N. Yoshinori, K. Md. Abdul Goffar, F. Begum, S. Kaijage, *Journal of Microwaves, Optoelectronics and Electromagnetic Applications (JMoe)* **6**, 44 (2007).
- [20] Y. Hou, F. Fan, Z.-W. Jiang, X.-H. Wang, S.-J. Chang, *Optik* **124**, 3095 (2013).
- [21] J. K. Valiunas, M. Tenuta, G. Das, *Journal of Sensors* **2016**, 9 (2016).
- [22] W. Jin, H. L. Ho, Y. C. Cao, J. Ju, L. F. Qi, *Optical Fiber Technology* **19**, 741 (2013).
- [23] Ahmmmed A. Rifat, Kawsar Ahmed, Sayed Asaduzzaman, Bikash Kumar Paul, R. Ahmed, *Computational Photonic Sensors*, Springer, Switzerland, 287 (2017).
- [24] S. Olyaei, A. Naraghi, V. Ahmadi, *Optik* **125**, 596 (2014).
- [25] M. Monir, H. Md. Imran, R. Tusher Kanti, U. Muhammad Shahin, S. M. A. Razzak, *Applied Optics* **54**, 8637 (2015).
- [26] S. Asaduzzaman, K. Ahmed, *Sensing and Bio-Sensing Research* **10**, 20 (2016).
- [27] A. A. Rifat, R. Ahmed, G. A. Mahdiraji, F. R. M. Adikan, *IEEE Sensors Journal* **17**, 2776 (2017).
- [28] W. L. Ng, A. A. Rifat, W. R. Wong, D. C. Tee, F. R. Mahamd Adikan, *Journal of Modern Optics* **64**, 1544 (2017).
- [29] R. A. Aoni, R. Ahmed, M. M. Alam, S. M. A. Razzak, *International Journal of Scientific & Engineering Research* **4**, (2013).
- [30] X. Tan, H. Zhang, J. Li, H. Wan, Q. Gue, H. Zhu et al., *Nature Communications* **11**, 5245 (2020).
- [31] D. Kwak, Y. Lei, R. Maric, *Talanta* **204**,
- [32] M. N. Petrovich, A. van Brakel, F. Poletti, K. Mukasa, E. Austin, V. Finazzi, P. Petropoulos, E. O'Driscoll, M. Watson, T. DelMonte, T. M. Monro, J. P. Dakin, D. J. Richardson, *Proc. SPIE* **6005**, 60050E (2005).
- [33] J. Broeng, D. Mogilevstev, S. E. Barkou, A. Bjarklev, *Optical Fiber Technology* **5**, 305 (1999).
- [34] H. Ebendorff-Heidepriem, P. Petropoulos, S. Asimakis, V. Finazzi, R. C. Moore, K. Frampton et al., *Opt. Express* **12**, 5082 (2004).
- [35] H. El Hamzaoui, Y. Ouerdane, L. Bigot, G. Bouwmans, B. Capoen, A. Boukenter, S. Girard, M. Bouazaoui, *Opt. Express* **20**(28), 29751 (2012).

---

\*Corresponding author: makouei@tabrizu.ac.ir